ACSNANO

www.acsnano.org

ARTICLE

Photoactive Control of Surface-Enhanced Raman Scattering with Reduced Graphene Oxide in Gas Atmosphere

Lu Zhou, Lauren Pusey-Nazzaro, Guanhua Ren, Ligang Chen, Liyuan Liu, Wentao Zhang, Li Yang, Jun Zhou,* and Jiaguang Han*

Cite This: *ACS Nano* 2022, 16, 577−587

Read Online

ACCESS | Metrics & More | Article Recommendations | Supporting Information

ABSTRACT: **Surface-enhanced Raman scattering (SERS) is an ultrahigh sensitive detection technique for a variety of research fields. Both electromagnetic and chemical enhancement mechanisms are generally considered to contribute simultaneously to SERS signals. However, it is difficult to actively control the enhancement of SERS signals after the substrate is fabricated, since tuning one or both of the aforementioned enhancement mechanisms remains an experimental challenge. Here, we propose a method for actively implementing the photoinduced modulation of SERS signals, which is that under UV irradiation, the Fermi level of graphene can be dynamically modulated due to the adsorption and desorption of gas molecules. The method is validated in gas atmospheres of O_2, CO_2, N_2, and air and also demonstrate its generality by different analytes. In addition, the method was successfully applied to the trace detection of pesticides on fruit peels in air environment, which show its practical implications in sensing.**

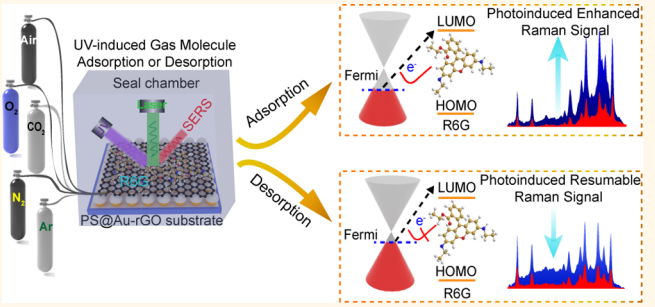

KEYWORDS: *surface-enhanced Raman scattering, reduced graphene oxide, ultraviolet light irradiation, adsorption, desorption*

As a powerful analytical technique allowing for ultrasensitive vibrational fingerprint detection of low concentration analytes, surface-enhanced Raman scattering (SERS) has stimulated widespread applications ranging from chemical analysis,[1,2] biological sensing,[3,4] environment monitoring,[5] to food safety.[6,7] Significantly enhanced SERS signals have made it a promising measurement indicator for characteristics of a variety of materials, thus offering the possibility of unveiling physical implication behind many phenomena. The dominant contributor to the enhancement of most SERS signals generally relies on the electromagnetic (EM) enhancement mechanism, where the excitation of localized surface plasmon resonances (LSPRs) can augment the pristine Raman signal by more than 10^8 times.[8,9] The other mechanism involved in signal enhancement is chemical (CM) enhancement, which originates from the charge transfer (CT) between analyte and substrate to result in increasing polarizability of the molecules, thereby enhancing the Raman scattering cross section.[10,11] The total SERS enhancement factor (EF) is then the product of the individual EM and CM enhancement. To implement the EM/CM dual-enhanced SERS substrate, researchers have paid their attentions on various hybrid systems composed of noble metal nanostructures and semiconductors, such as Au/Ag-TiO_2,[12−14] Fe_3O_4/SiO_2/ZnO/Ag,[15] Ag-ZnO,[16] and so on. Although ultrahigh enhancement has been achieved successfully, in most circumstances the enhancement of SERS signals of studied analytes is typically fixed once the substrate has been prepared. However, CM enhancement requires the Fermi level of the substrate to match with the highest occupied molecular orbital (HOMO) and lowest unoccupied molecular orbital (LUMO). The mismatched surface energy levels of the composite nanostructure and the analyte would significantly reduce the CM enhancement due to limiting CT. Therefore, tuning the energy level alignment of nanostructures to better match the energy level of analyte is crucial to improve the CM enhancement effect.

In this regard, graphene is a great candidate for SERS substrate by improving CM enhancement through enabling CT with analytes. A number of factors responsible for

Received: September 2, 2021
Accepted: December 14, 2021
Published: December 20, 2021

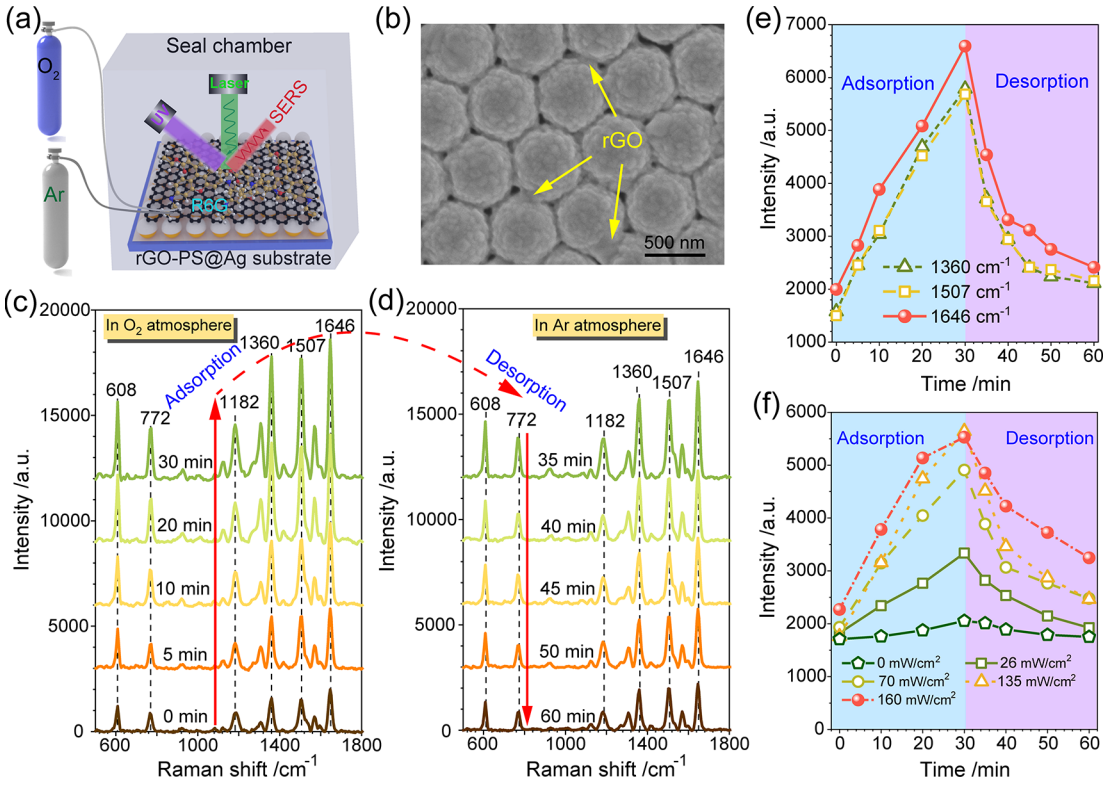

Figure 1. Modulation of SERS signals in O_2 atmosphere. (a) Schematic diagram of *in situ* and real-time Raman measurement of the rGO-PS@Ag substrate under UV-irradiation in O_2 or Ar atmosphere. Note: UV light source is introduced on the side of the Raman laser. (b) SEM image of the rGO-PS@Ag substrate. SERS spectra of the R6G adsorbed on the rGO-PS@Ag substrate under UV irradiated (c) in O_2 atmosphere (adsorption), (d) subsequent exposure of the sample to Ar atmosphere (desorption), and (e) corresponds to temporal evolution of the SERS intensities of peaks at 1360, 1507, and 1646 cm^{-1}. (f) Time-evolution of SERS intensities of the peak at 1360 cm^{-1} for R6G adsorbed on the PS@Ag-rGO substrate irradiated with different irradiance intensities of 365 nm light.

graphene-based SERS activity have been discussed, such as the distance between molecules and graphene, different vibrational modes, the Fermi level of graphene, and laser excitation energies.[17−20] Among them, tuning the Fermi level of graphene has been proven to be an effective strategy for obtaining the better SERS activity. The Fermi level of graphene can be tuned by modifying the graphene surface, that is, by exploiting p-type and n-type doping,[21] UV/ozone treatment,[22] chemical oxidation,[23] or electrical field effect,[24−26] thus facilitating CM-based enhancement by better matching the energy levels of the analytes. Huh *et al.* prepared a large SERS-active graphene substrate by UV/ozone oxidation treatment, and they found this oxidation along p-doping can result in very high SERS signal.[22] Yang *et al.* developed a dual-enhanced Raman scattering substrate by using graphene-plasmonic hybrid nanoarray and realized CM-based SERS signal enhancement by tuning the oxidation levels of graphene oxide.[23] Zhang's group has demonstrated that the Raman scattering intensities of adsorbed molecules can be tuned to be stronger or weaker under different atmospheres by applying the external bias, where the Femi level of graphene could be tuned electrically.[25] They also found that the Raman modulation ability is different due to the difference in the range of Fermi level modulation under different types of doping atmospheres.[26] Thus far, we could find that besides a high EM enhancement, making an excellent performance of dual-enhanced SERS substrate with methods to actively tune CM enhancement is of great interest.

In this work, we propose and demonstrate an active control strategy for the enhancement of SERS signals. Considering the demand of tailoring substrate properties, our chosen SERS substrate consists of an Ag-coated polystyrene (PS@Ag) nanoarray covered by a self-assembled reduced graphene oxide (rGO) film, denoted as rGO-PS@Ag substrate. The results show that the SERS signals of analytes adsorbed onto the rGO-PS@Ag substrate can be actively manipulated through UV-induced adsorption and desorption of surrounding gas molecules. The rGO is crucial in our ability to adjust SERS signals, since the Fermi level of rGO can be actively manipulated by UV-induced gas molecular adsorption (of O_2, CO_2, and N_2) or desorption (by Ar), which in turn regulates the CT between the substrate and analytes, thereby modulating the SERS signal. For practical applications, the proposed control methodology is implemented for various analytes in dry air and also used to detect the residual pesticides present on fruit peels.

RESULTS AND DISCUSSION

Sample Preparation. The SERS substrate was fabricated using the Langmuir−Blodgett method, magnetron sputtering, and self-assembly at the water−air interface (see Figure S1) and is comprised of a PS@Ag nanoarray and a self-assembled rGO film (Figure 1a). The morphology and composition of the rGO-PS@Ag substrate were characterized by scanning electron microscopy (SEM), Raman spectroscopy, and X-ray photoelectron spectroscopy (XPS) (Figures S2−S4). The self-assembled rGO film covers on the surface of PS@Ag nanoarray

https://doi.org/10.1021/acsnano.1c07695
ACS Nano 2022, 16, 577−587

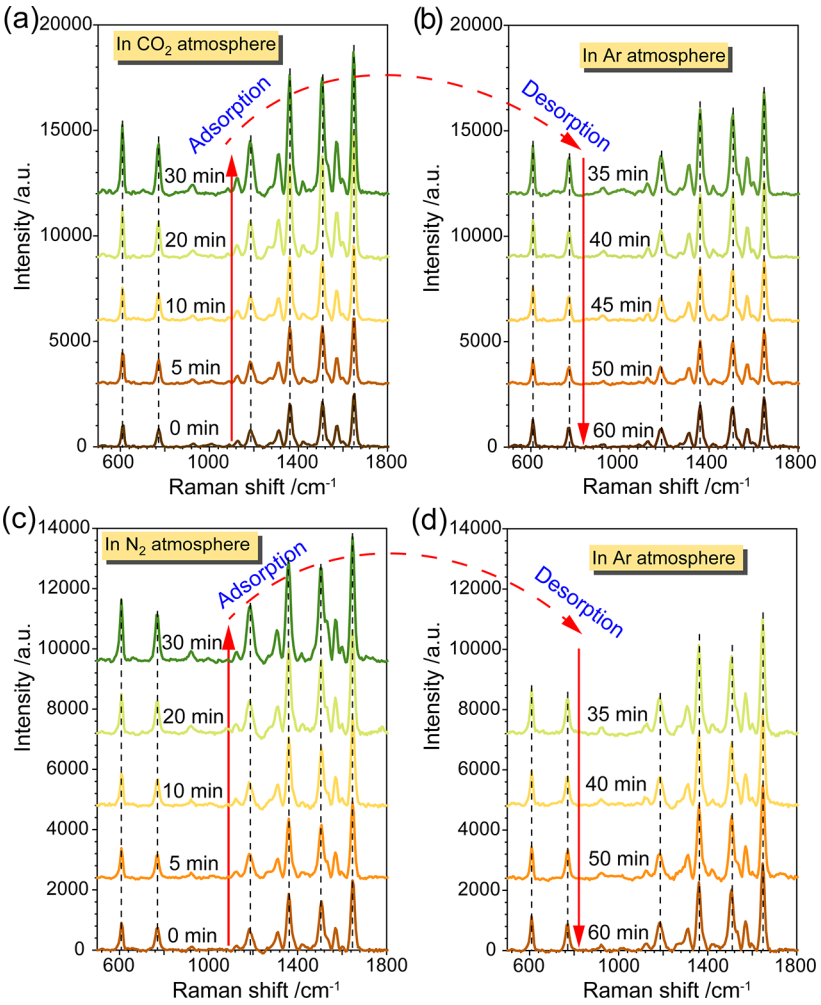

Figure 2. Modulation of SERS signals in other gas atmospheres. SERS spectra of the R6G adsorbed on the rGO-PS@Ag substrate under UV irradiated in (a) CO_2 and (c) N_2 atmosphere (adsorption) and (b and d) subsequent exposure of the rGO-PS@Ag substrate to Ar atmosphere (desorption).

can be clearly seen in Figure 1b, as marked by arrows. The appearance of Raman peaks of D and G bands, the change of chemical state, and the binding energy all indicate that the rGO-PS@Ag substrate was successfully prepared. A more detailed analysis can be found in Section S1 of Supporting Information.

Characterization of the SERS Sample. Figure 1a is a schematic depicting *in situ* and real-time Raman measurement for rhodamine 6G (R6G) molecule adsorbed onto the rGO-PS@Ag substrate under UV irradiation (365 nm, 135 mW/cm^2) in O_2 or Ar atmosphere. The SERS characteristics of the sample are measured under a Raman laser with a wavelength of 532 nm, power density of 7.8 W/cm^2, and an integration time of 2 s. The UV irradiation time-dependent SERS spectra of R6G molecule adsorbed on the substrate in O_2, subsequently exposed to an Ar atmosphere, are shown in Figure 1c,d, respectively. The main SERS peaks observed at 1182, 1306, 1360, 1507, and 1646 cm^{-1} are attributed to the aromatic C−C stretching vibrational modes, and peaks at 608 and 772 cm^{-1} are due to in-plane vibrations of C−C−C bonds and out-of-plane vibration of C−H bonds, respectively.[27,28] As the UV irradiation time is increased from 0 to 30 min in the O_2 atmosphere, the SERS signal of R6G is significantly enhanced, and the corresponding EF undergoes a pronounced modulation nearly 4-fold, as illustrated in Figure 1c. When we replace O_2 atmosphere with an Ar atmosphere, the SERS signal is decreased to <50% within the first 10 min of exposing in Ar. The signal is further reduced and almost completely recovered to the original one with a continuous Ar purge, as shown in Figure 1d. Figure 1e depicts the modulation process by collecting the intensities of the SERS peaks at 1360, 1507, and 1646 cm^{-1} varying with the UV irradiation time in the O_2 and Ar atmospheres. In this modulation process, the adsorption of O_2 onto the substrate enhances the SERS signal, while the desorption process recovers the signal. Evidently, a reversible modulation of SERS signal intensity is realized through UV-induced adsorption and desorption of O_2 atmosphere. We noticed that the SERS signals reached the maximum at about 30 min UV exposure in O_2 atmosphere and then remained unchanged. If the UV illumination was more than 40 min (Figure S5), the signals become weaker due to the UV-induced damage of the substrate. To avoid the damage of the substrate, the optimum irradiation time (30 min) was chosen in the following experiments. During the experiment, we also noticed that the modulation is substantially influenced by the irradiation intensity of UV light.[29] As shown in Figure 1f (also see Figure S6), when the UV irradiation intensities are increased from 0 to 160 mW/cm^2, it not only speeds up the

https://doi.org/10.1021/acsnano.1c07695
ACS Nano 2022, 16, 577−587

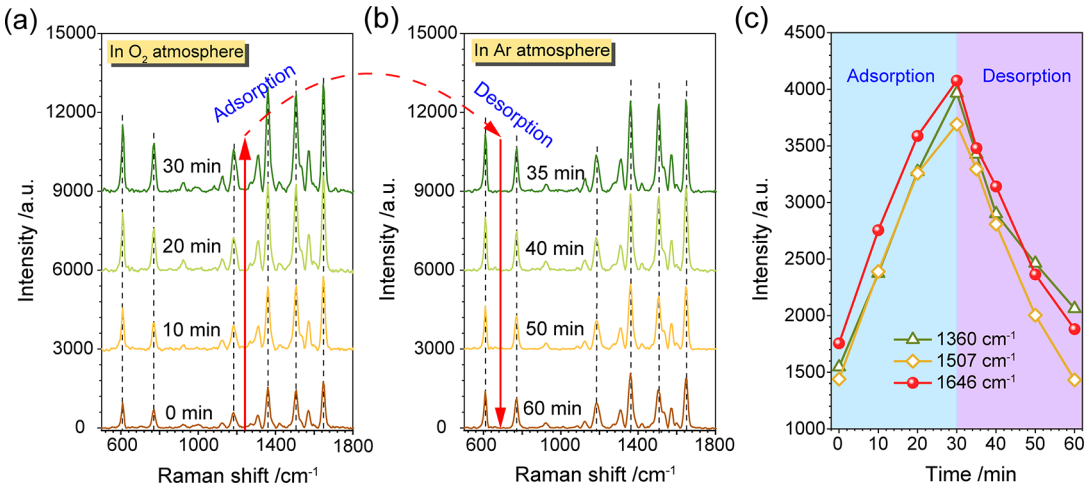

Figure 3. Modulation of SERS signals on monolayer graphene. SERS spectra of the R6G adsorbed on the graphene-PS@Ag substrate under UV irradiated in (a) O_2 atmosphere (adsorption), (b) subsequent exposure of the substrate to Ar atmosphere (desorption), and (c) corresponds to temporal evolution of the SERS intensities of peaks at 1360, 1507, and 1646 cm^{-1}.

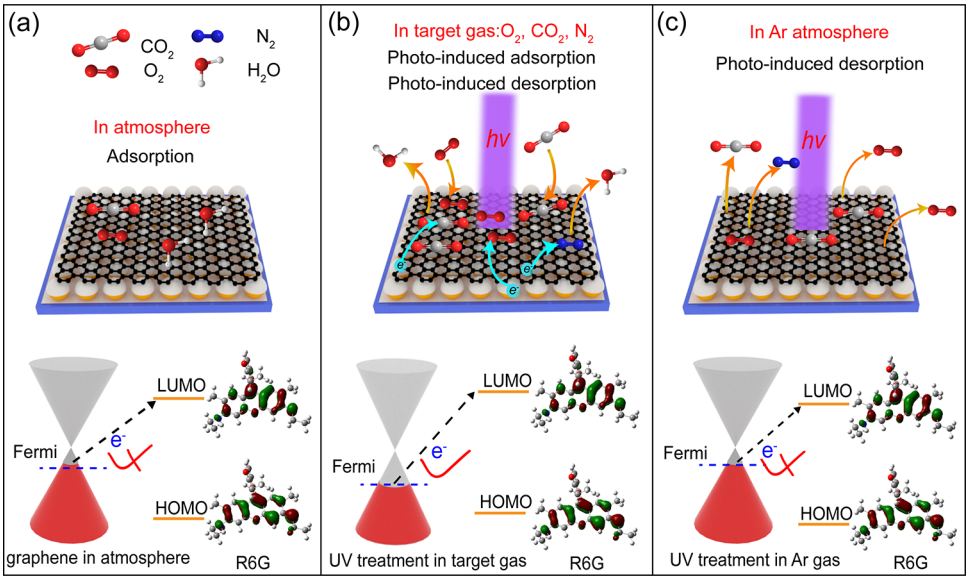

Figure 4. Modulation mechanism of SERS performance. Photoinduced gas molecular adsorption and desorption on the substrate, corresponding to change in the Fermi level of graphene, which either promotes or inhibits CT between the substrate and R6G.

adsorption and desorption processes but also affects the modulation capability. When the intensity of UV light is more than 135 mW/cm^2, the influence of UV light approaches saturation for the enhancement of SERS signals.

We proceed to study of the modulation effect in CO_2 and N_2 atmospheres. Figure 2a–d shows the modulation of the SERS signal of R6G due to the UV-induced adsorption and desorption of CO_2 and N_2. We note that the modulation of the SERS signal in CO_2 atmosphere is almost the same as the case in the O_2, and more dramatic than that in the N_2 atmosphere. This is because as electron acceptors, O_2 and CO_2 molecules prefer to obtain electrons from rGO, thereby tuning the Fermi level of rGO to facilitate the CT with analyte, the net result being an enhanced SERS signal.[29] To compare the modulation behavior of different gas atmospheres, we calculate the EFs for each respective atmosphere, listed in Table S1 (see detailed information in Section S2 of Supporting Information). We find that the rGO-PS@Ag substrate displays substantial SERS activity, and by UV irradiation in the O_2 (CO_2) atmosphere, the EF is increased from 1.77×10^6 (1.14×10^6) to 6.75×10^6 (4.07×10^6). In both such atmospheres, a near 4-fold enhancement is achieved. Even in N_2 atmosphere, where the ability to accept electrons is far less than O_2 and CO_2, we observe that a 1.7-fold enhancement can still be obtained. It indicates that the gaseous environment plays an important role in actively controlling SERS performance.

To further explore the effect of the UV-induced adsorption and desorption of gas molecules on the rGO-PS@Ag substrate, we measured the SERS spectra of the substrate under UV irradiation in O_2 atmosphere and subsequent exposure to Ar atmosphere, as shown in Figure S8. It can be seen that in O_2 atmosphere, the UV illumination results in the increase of the ratio of D and G band (I_D/I_G) as well as the full width at half-maximum (W_h) of D and G band of the rGO. This is because the UV-induced adsorption of O_2 molecules gives rise to the doping of rGO film.[30] On the other hand, in Ar atmosphere, UV irradiation induces the decrease of I_D/I_G and W_h and finally returns back to the original point due to the desorption

https://doi.org/10.1021/acsnano.1c07695
ACS Nano 2022, 16, 577–587

of O_2 molecules. Thus, we could see that the rGO can be reversibly doped by UV-induced adsorption and desorption of gas molecules.

Moreover, we also investigated the modulation effect on monolayer graphene, which covered on PS@Ag nanoarray. Figure 3a,b shows the modulation of the SERS signal of R6G adsorbed on graphene-PS@Ag substrate under UV-irradiated in O_2 atmosphere, subsequently exposed to an Ar atmosphere. We observed that the modulation of the SERS signal on graphene-PS@Ag substrate in O_2 atmosphere is almost the same as the case on the rGO-PS@Ag substrate. Figure 3c depicts the modulation process by collecting the intensities of the SERS peaks at 1360, 1507, and 1646 cm^{-1} varying with the UV irradiation time in the O_2 and Ar atmospheres. In this modulation process, the adsorption of O_2 onto the graphene enhances the SERS signal, while the desorption process recovers the signal to the original. To compare their modulation capability, we calculate the EF for both substrates and listed in Table S1 (see detailed information in Section S2 of Supporting Information). The SERS signal of R6G on graphene presents a nearly 3-fold enhancement, which is less than that on rGO (nearly 4-fold), as the UV irradiation time is increased from 0 to 30 min in the O_2 atmosphere. This is because the defect or functional groups in rGO act as high-energy absorption sites, which can increase the selectivity and sensitivity to gas adsorption.[31] In view of all the above results and discussions, the modulation effect of SERS signal can also occur on graphene by photoinduced adsorption and desorption of gas molecules.

Modulation Mechanism. To explore the origins of the active modulation behavior of SERS signal observed above, we analyze both UV-induced gas molecular adsorption and desorption processes.[32] Figure 4 shows a schematic of the photoactivated adsorption and desorption of gas molecules on the substrate, and subsequent changes to the Fermi level of graphene. Without any treatment, the initial monolayer graphene is p-doped due to oxygen and water molecules present in the ambient air. In this case, the CT between graphene and the studied analytes is limited due to a mismatch of energy levels (Figure 4a). When the substrate is exposed to the target gas atmosphere and UV irradiation is applied, the photogenerated electron−hole pairs appear in the graphene surface. In effect, a photogenerated electron $e^-(h\nu)$ can combine with O_2 (CO_2) molecules, enhancing the p-doped nature of graphene (Figure 4b), in accordance with the following reaction:[33−35]

$$O_2(\text{ads}) + e^-(h\nu) \rightarrow O_2^-(\text{ads}) \quad (1)$$

$$CO_2(\text{ads}) + e^-(h\nu) \rightarrow CO_2^-(\text{ads}) \quad (2)$$

As gas molecules are adsorbed onto the surface of the substrate, the p-doped properties of graphene are enhanced due to electron consumption by the external atmosphere. The decreased Fermi level of graphene is now much better matched to the orbital energy of the studied analyte, which facilitates the CT between R6G and graphene, as shown in Figure 4b. Subsequently, when the O_2 (CO_2) gas molecules are withdrawn, the equilibrium achieved in eqs 1 and 2 is disturbed. The photoinduced adsorption of O_2^- (CO_2^-) will revert to O_2 (CO_2) and then will be desorbed from the substrate according to the following equations:[35]

$$O_2^-(\text{ads}) + h^+(h\nu) \rightarrow O_2(\text{gas}) \quad (3)$$

$$CO_2^-(\text{ads}) + h^+(h\nu) \rightarrow CO_2(\text{gas}) \quad (4)$$

This process is illustrated in Figure 4c. In effect, tuning the Fermi level of graphene through adsorption and desorption of gas molecules can reversibly modulate CM enhancement in the SERS signal.[23,26]

Meanwhile, the graphene-based SERS enhancement rules can be concluded from other two-dimensional graphene analogs:[19,36]

$$\hbar\omega_0 = \text{LUMO} - \text{HOMO} \text{ or } \hbar\omega_0 = \text{LUMO} - \text{HOMO} + \hbar\omega_q \quad (5)$$

$$\text{Fermi} = \text{HOMO} \pm \hbar\omega_q \text{ or Fermi} = \text{LUMO} \pm \hbar\omega_q \quad (6)$$

$$\hbar\omega_0 = \text{Fermi} - \text{HOMO} \text{ or } \hbar\omega_0 = \text{Fermi} - \text{HOMO} + \hbar\omega_q \quad (7)$$

$$\hbar\omega_0 = \text{LUMO} - \text{Fermi} \text{ or Fermi} = \text{LUMO} - \text{Fermi} - \hbar\omega_q \quad (8)$$

where $\hbar$ is the reduced Planck's constant, ω_0 is the frequency of incident Raman laser, and ω_q is the frequency of scattered photons. Eq 5 is related to the resonance between the molecular electronic transition with either the incident light or the scattering light, respectively, and eq 6 is the condition of optimal resonance for the Fermi energy. The optimal resonance occurs when the Fermi energy is above or below one of the molecular electronic levels by exactly the phonon energy. Moreover, eqs 7 and 8 are the conditions of electronic transition between the molecule and graphene. It happens when the laser energy matches the energy difference between the Fermi energy of graphene and the HOMO or LUMO states of the molecule plus or minus the scattering phonon energy. Accordingly, an enhanced Raman signal is strongly dependent on the resonance between the molecular electronic transitions and the incident light; namely, the laser energy should match the energy difference between the Fermi level and the state energy of the HOMO or LUMO of the molecules.

Moreover, considering the competition of analytes (such as R6G) and gas molecules for adsorption sites on the substrate, the time-evolution SERS spectra of the different concentrations of R6G molecules adsorbed on the substrate under UV irradiated in O_2 atmosphere were measured and the results were shown in Figure S9. We can find that as the content of R6G molecules adsorbed on the substrate increase, the adsorption sites of gas molecules (such as O_2 molecule) decrease, which in turn resulting in reducing the enhancement of the SERS signal. The detailed analysis is shown in Section S3 of Supporting Information. Furthermore, we have also studied the relationship between the modulation of SERS signal and the adsorption amount of O_2 by changing the Ar/O_2 mixing ratios in atmosphere. Figure S10 shows the measured SERS signals at various Ar/O_2 mixing ratios under UV irradiation. The results indicate that the adsorption amount of O_2 significantly influences the CT and thus influences the modulation of SERS signals (see Section S4 in Supporting Information).

To confirm the working mechanism, we study the correlation of the Fermi level of graphene and the adsorption of O_2 molecules using density functional theory (DFT) calculations. The band structures and density of states of intrinsic graphene and the graphene with adsorption of O_2 molecules are shown in Figure 5a,b, respectively. Compared to

https://doi.org/10.1021/acsnano.1c07695
ACS Nano 2022, 16, 577−587

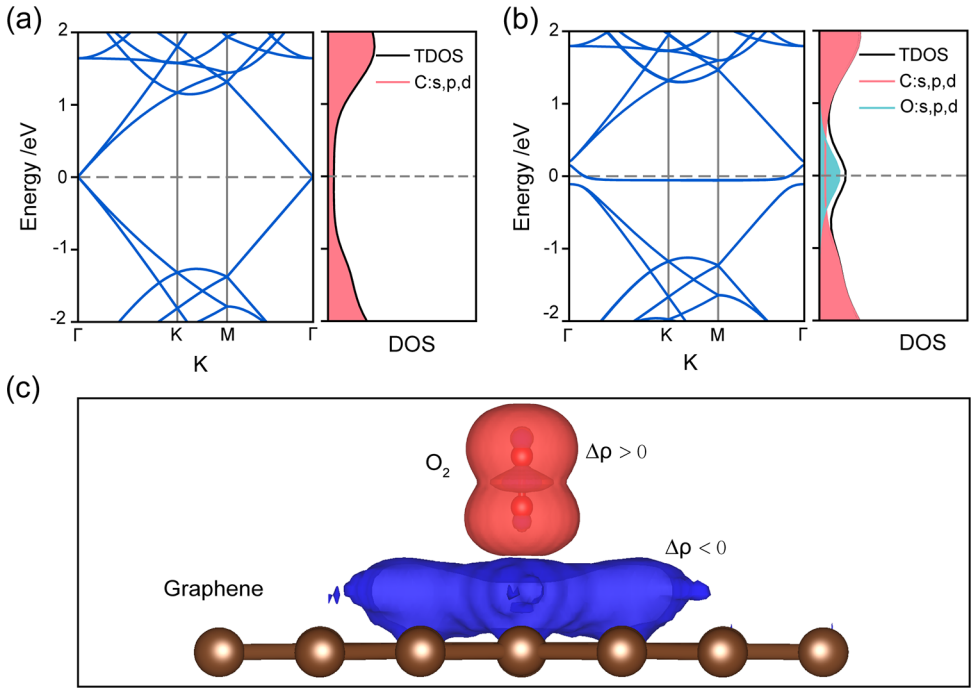

Figure 5. DFT calculation. The band structure and density of states of (a) intrinsic graphene and (b) graphene with adsorption of O_2 molecule. (c) Isosurface of the induced charge density of the graphene adsorbed with O_2 molecule. Red regions show where CT is positive, and blue where it is negative.

the intrinsic graphene, we found that the Fermi level of graphene in the presence of O_2 moves down into the valence band, effectively hole doping in the system. This decrease in the Fermi level is of order 180 meV, due to the presence of O_2 in our simulations. In order to verify the possible CT, we plotted the isosurfaces of the induced charge density ($\Delta\rho$) of graphene adsorbed with an O_2 molecule in Figure 5c. $\Delta\rho > 0$ (red) indicates positive CT, while $\Delta\rho < 0$ (blue) indicates negative CT. It shows clearly that the O_2 molecule gains charge when it is adsorbed on graphene surface. Our calculations demonstrate that CT occurs from neighboring C atoms within the C_6 ring of graphene to the adjacent O_2 molecule, resulting in p-type doping of graphene with an estimated hole density of 6×10^{12} cm^{-2}. The calculation result agrees with the working mechanism proposed above.

Modulation of SERS Signals in Air. Considering the practical application environment, we study the modulation behaviors of the SERS signal specifically in ambient air. As shown in Figure 6a,b, upon UV irradiation in ambient air, the SERS signals of R6G adsorbed on the rGO-PS@Ag substrate exhibit enhancement as the irradiation time increases. Followed by a purge of Ar, the SERS signal is reduced but not completely restored to the original intensity, which may be due to the water vapor present in the moisture-rich ambient air. So, we expose the sample to dry air instead of moisture-rich ambient air, and therewith purged by Ar atmosphere, a reversible modulation of the SERS signal is arrived, as illustrated in Figure 6c,d. Furthermore, we compare the tunability of the proposed platform in the ambient air and in dry air by repeating the modulation cycle. As shown in Figure 6e (also see Figures S11 and S12), we find that in ambient air, the SERS signal is decreased dramatically after two cycles. This is due to the oxidizing of underlying Ag and rGO films by OH radicals generated by UV light under moisture-rich ambient conditions.[37,38] However, in the dry air, the SERS signal shows a reversible modulation behavior, as represented in Figure 6e. Figure 6f,g also demonstrates that the photoinduced SERS enhancement in the dry air is less than that in O_2 and CO_2 atmospheres, but higher than that in an N_2 atmosphere.

In addition, we investigate the modulation behaviors of the SERS signal using a number of other analytes adsorbed on the rGO-PS@Ag substrate. Figure 7a–c shows the SERS spectra of crystal violet (CV), 4-mercaptobenzoic acid (4MBA), and 4-nitrothiophenol (4NTP) molecules before and after the 30 min UV irradiation in dry air, respectively. We find that SERS spectra of these three analytes are enhanced after 30 min UV illuminate in dry air, similar to our results obtained for R6G. The EFs for all four Raman reporters on the rGO-PS@Ag substrate before and after UV irradiated are calculated and listed in Table S2. One can find that for different analyte molecules adsorbed on the rGO-PS@Ag substrate, UV treatments increase the values of EF, but there is a difference of SERS enhancement efficiency for different analytes. That is, a consequence of Raman enhancement is strongly related to the molecular energy levels of the particular analyte.[17,19] In accordance with our DFT calculations, the orbital energy level diagram and their HOMO/LUMO energies of four molecules are shown in Figure 7d. The four molecules possess HOMO/LUMO energies of −5.70/−3.40 eV,[39] −6.00/−4.1 eV,[18] −6.44/−2.3 eV,[40] and −5.8/−2.45 eV,[41] respectively. The larger SERS signals enhancement of R6G and 4NTP is attributed to the photon energy of 532 nm laser, which is closer to the energy difference between the Fermi level of rGO and the HOMO/LUMO levels of R6G and 4NTP molecule, which can effectively induce CT between these molecules and rGO. However, the mismatched energy levels of rGO and the analytes CV and 4MBA can significantly reduce the CM-based SERS enhancement by limiting CT. Consequently, for different analytes, the modulation efficiencies of the SERS signals are different.

https://doi.org/10.1021/acsnano.1c07695
ACS Nano 2022, 16, 577−587

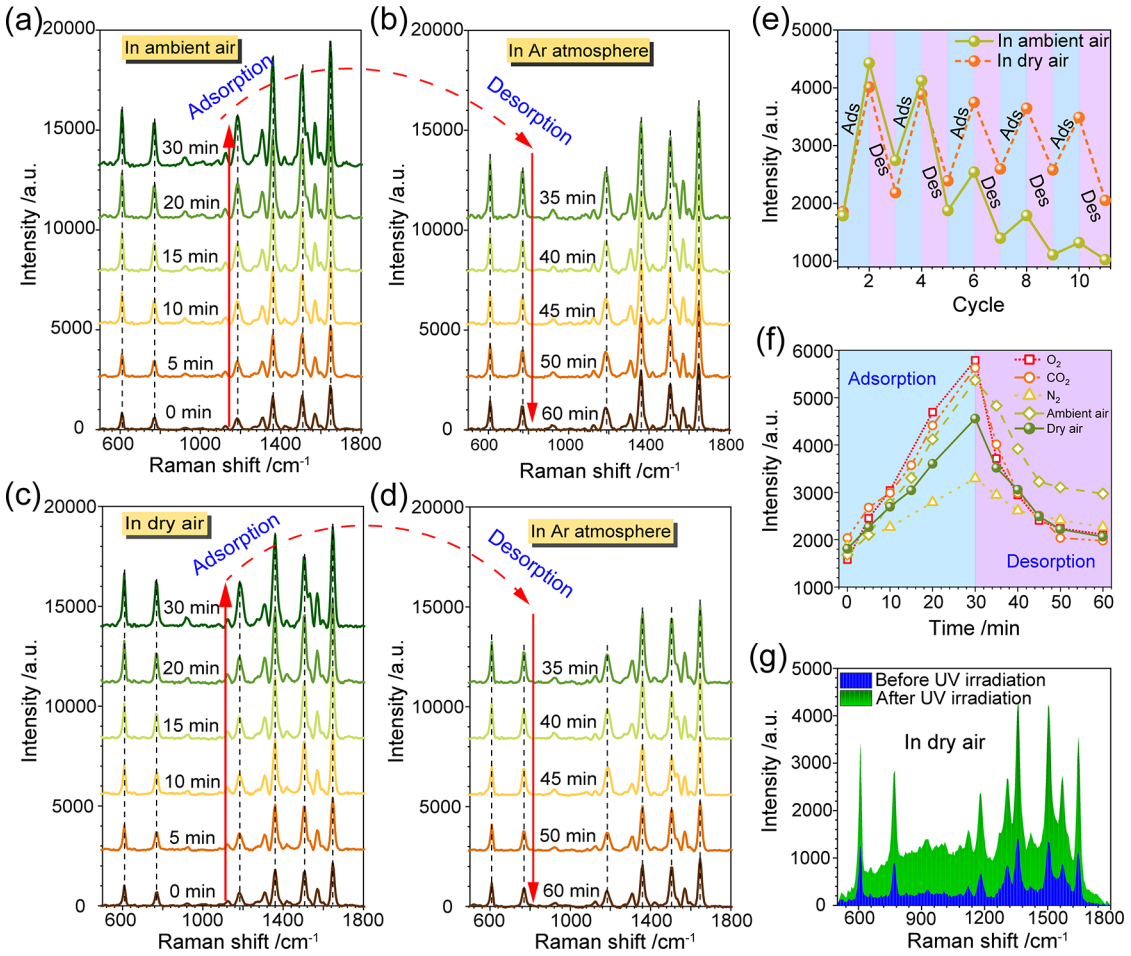

Figure 6. Modulation of SERS signals in air. SERS spectra of the R6G adsorbed on the rGO-PS@Ag substrate under UV irradiated in (a) ambient air and (c) dry air (adsorption) and (b and d) subsequent exposure of the rGO-PS@Ag substrate to Ar atmosphere (desorption). (e) The SERS intensities of peaks at 1360 cm^{-1} for R6G adsorbed on the rGO-PS@Ag substrate by alternating ambient air or dry air (adsorption) and Ar atmosphere (desorption) under UV irradiation. (f) Time evolution of SERS intensities of the peak at 1360 cm^{-1} for R6G adsorbed on the rGO-PS@Ag substrate irradiated by UV light in different atmosphere, such as O_2, CO_2, ambient air, dry air, and N_2. (g) SERS spectra of R6G adsorbed on the substrate before and after 30 min UV irradiation of in dry air.

Practical Application. In our present work, the reproducibility of the rGO-PS@Ag substrate with excellent SERS signal enhancement is explored for its potential application in biosensing. For different batches of rGO-PS@Ag substrates as well as different locations in the same substrate, the SERS modulations are also studied, as shown in Figures S13 and S14 (see Section S5 in Supporting Information). It confirms that the rGO-PS@Ag substrate has a good repeatability and reliability, which can satisfy the requirement of accurate trace detection. The following is a practical example of the rGO-PS@Ag substrate as a SERS detection platform. As is well-known, methyl parathion (MP) is a prototypical organophosphorus insecticide and has been widely applied in many agriculture fields, while the MP residues cause a grave food safety problem for humans. For this reason, it is of great importance to accurately detect the presence of MP residues on agricultural products, and we apply our proposed techniques of SERS signal modulation and enhancement for this purpose as follows. First, MP solutions of different concentrations (10^{-1} to 10^{-6} mg/mL) were dropped on the rGO-PS@Ag substrate, and their SERS spectra were recorded before and after UV illumination in dry air. Expectedly, as demonstrated in Figure 8a, the SERS signal of MP is greatly enhanced at all test concentrations upon UV illumination. The main characteristic peaks discernible from the entire spectrum are located at 864, 1111, 1274, 1328, and 1590 cm^{-1} and are assigned to ν(P−O), ν(C−N), ν(C−O), and ν(N−O) and phenyl stretch vibrational modes, respectively.[42,43] We choose the SERS peak of greatest intensity, located at 1328 cm^{-1} in Figure 8a, as the calibration band with the goal of analyzing the correlation between the SERS intensity and MP concentration. From Figure 8c, one may see that the rGO-PS@Ag substrate before and after UV illumination demonstrates low limits of detection (LODs)[44] of MP are 1.54×10^{-6} mg/mL and 8.31×10^{-7} mg/mL, respectively, which are lower than that of PS@Ag nanoarray (see Figure S15). The LOD of MP adsorbed on the rGO-PS@Ag substrate with UV treatment is about 2-fold lower than that without treatment, and it is lower than the minimal residue limit of 0.2 mg/kg in fruits established by the European Union (EU) and Food and Agriculture Organization (FAO).[45] In order to investigate the feasibility, the apple and pear peels were chosen to extract MP for the SERS-based detection. Ten μL of MP solution with 10^{-4} mg/mL was dropped onto the peels of the fruits and evaporated naturally at room temperature for 1 day. Then the MP from the pretreated peels was extracted as following: (1) drop methanol solution

https://doi.org/10.1021/acsnano.1c07695
ACS Nano 2022, 16, 577−587

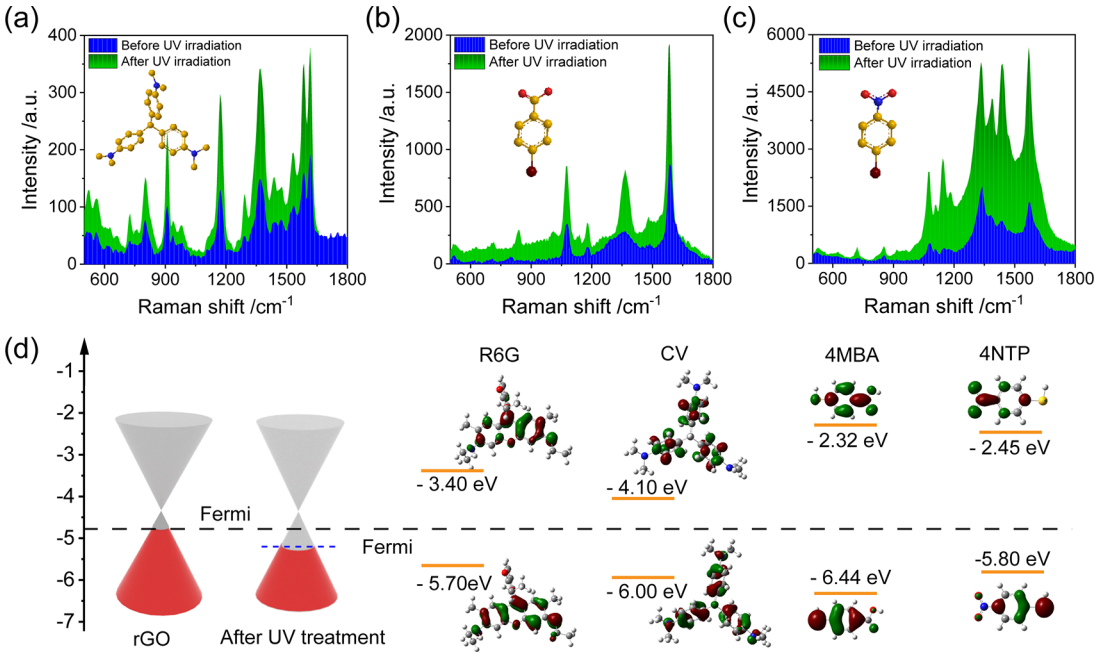

Figure 7. Modulation behavior of SERS signals for different analytes. SERS spectra of (a) CV, (b) 4MBA, and (c) 4NTP adsorbed on the rGO-PS@Ag substrate before and after UV irradiation in dry air. (d) The Fermi levels of rGO before and after UV treatment, the HOMO/LUMO energy levels of R6G, CV, 4MBA and 4NTP and corresponding the orbital energy level diagram.

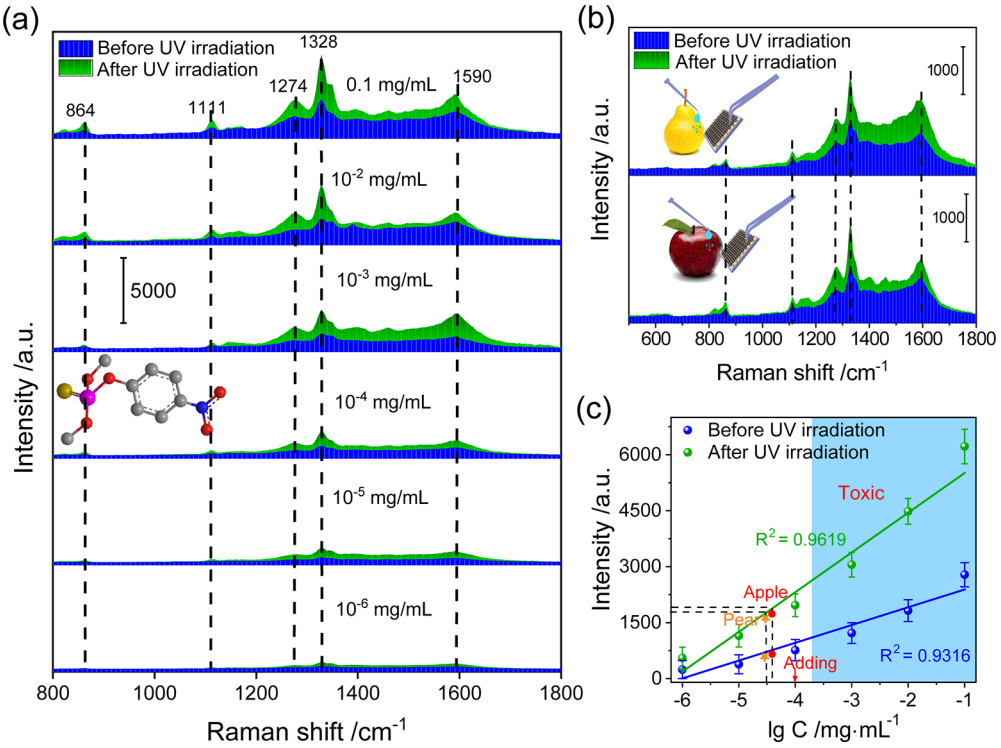

Figure 8. Pesticide residue detection on fruit peels. (a) SERS spectra of MP with different concentrations (from 10^{-1} to 10^{-6} mg/mL) adsorbed on the rGO-PS@Ag substrate before and after UV irradiation in dry air. (b) SERS spectra of MP extracted from the pear and apple peels. The inset images depict the extraction of MP from fruits peels. (c) Corresponding dose−response curves of the peak intensity at 1328 cm^{-1} before and after UV irradiation in dry air.

on the surface of the pretreated peel to dissolve the MP; (2) then grasp the substrate with tweezer and gently swab the place where the methanol solution was just dropped; and (3) repeat the previous two steps 2−3 times to ensure that the MP on the surface of the peel is extracted as much as possible (see Supplementary Video S1). Typically, the SERS spectra of MP from sampling of apples and pears show the characteristic peaks at a concentration of 10^{-4} mg/mL before and after UV irradiation in dry air (Figure 8b). In fact, the final concentration of MP is $<10^{-4}$ mg/mL because not all of the MP is redissolved in ethanol during sampling process, but the concentration lower than that the maximum residue level

https://doi.org/10.1021/acsnano.1c07695
ACS Nano 2022, 16, 577−587

prescribed by EU and FAO is still detected (see Figure 8c). In order to verify our proposed SERS-based detection method, we also measured the contents of MP by using high-performance liquid chromatography (HPLC) for the same sample. The results are shown in Figure S16. We could see for the same sample that the results measured from SERS are in good agreement with those measured from the HPLC.

CONCLUSION

In summary, we have successfully constructed a photoactively tunable SERS platform by combining a PS@Ag nanoarray with a self-assembled reduced graphene oxide film. Upon UV illumination, the rGO-PS@Ag substrate gives rise to an enhanced SERS signal by adsorbing gas molecules from the surrounding atmosphere. Subsequently, the SERS signal can be restored to its original intensity by desorbing of gas molecules. The active tuning of the SERS signal is attributed to the change of Fermi level of the rGO controlled by UV-induced adsorption and desorption of gas molecules, which modulates the CT between the substrate and analytes. From a practical perspective, the ability and generality of our proposed method is also demonstrated in an atmosphere of air and using a variety of analytes. As a typical example, we show how our technique may be useful in the field of biosensing in the detection of pesticide residues on fruit peels. The results highlight the ability to dynamically control SERS signal enhancement and expand SERS capabilities to future sensing applications. It is helpful in the understanding of the numerous underlying mechanisms responsible for the SERS enhancement.

METHODS

Fabrication of the rGO-PS@Ag Substrate. The rGO-PS@Ag substrate was fabricated by a process that consisted of the following two steps, as shown in Figure S1. First, the PS@Ag nanoarray was prepared using the Langmuir−Blodgett (L-B) method and magnetron sputtering. As a typical hydrophilic treatment,[46] the clear silicon wafer was placed in a solution of H_2O:H_2O_2:NH_4OH (5:1:1 by volume) held at 60 °C for 30 min, followed by an overflow rinse in running DI water and drying by nitrogen gas. Next, 300 μL of PS nanosphere suspension (3 wt %) diluted by ethanol was gently injected on the air/water interface in a beaker full of water using a mechanical syringe pump at a rate of 0.3 mL·h^{-1}. Then, with the help of sodium dodecyl sulfate (5 μL, 0.5 wt %), the hexagonally close-packed monolayer of PS nanospheres was formed and transferred to the hydrophilic silicon wafers by picking up the wafers from the water. Afterwards, a 200 nm Ag film was deposited onto the surfaces of PS nanoarray by sputtering an Ag target (99.99%) in a radio frequency magnetron sputtering system, operated at 0.3 Pa and a power of 50 W in ambient Ar, and the PS@Ag nanoarray was well fabricated. Second, the self-assembly of reduced graphene oxide (rGO) films at the liquid/air interface is illustrated in step two of Figure S1. Typically, 500 μL of rGO suspensions (1 mg/mL, $V_{water}/V_{ethanol}$ = 1:1) was gently injected on the air/water interface in a beaker full of DI water, and ethanol quickly spread on the DI water surface owing to the Marangoni effect.[47,48] Then, as the rGO spread and ethanol evaporated, the graphene flakes would collide and bind with each other via π−π interactions to form rGO film on the surface of DI water.[47,49] Finally, the assembled rGO films were transferred to the PS@Ag nanoarray by picking up the substrates from the water.

SERS Spectroscopy Measurement. The SERS spectra were collected using a Raman spectrometer (QE Pro, Ocean Optics) equipped with a microscope with a 50× objective lens at the excitation wavelength of 532 nm. Ten μL of analyte (R6G, CV, 4MBA, and 4NTP) solution (1 mM) was dropped onto the rGO-PS@Ag substrate and then placed into seal chamber to measure SERS spectra under UV light irradiation by blowing target gas.

Computational Details. First-principles simulations were performed using the Vienna *ab initio* simulation package,[50] and the local density approximation was employed in all calculations of the ground-state properties of oxygen molecules attached to graphene. We sampled reciprocal space using a Monkhorst−Pack grid of 9 × 9 × 1 *k*-points and an energy cutoff of 400 eV for our plane-wave basis set. To avoid spurious interactions between individual slabs in our simulations, the vacuum distance between slabs was set to be 20 Å. Structural optimizations were performed to a force tolerance of 0.01 eV/Å. In all calculations, we used a 6 × 6 supercell, containing 72 carbon atoms and a single O_2 molecule.

ASSOCIATED CONTENT

Supporting Information

The Supporting Information is available free of charge at https://pubs.acs.org/doi/10.1021/acsnano.1c07695.

SEM images, Raman and XPS spectra; irradiation time-dependent SERS spectra; irradiance-dependent modulation of SERS signal; calculation of the SERS enhancement factors; the evolution of Raman spectra of rGO under UV irradiation in O_2 atmosphere and Ar atmosphere; concentration-dependent modulation of SERS signals; the influence of different Ar/O_2 ratios on the modulation of SERS signals; reversibly cycled modulation; evaluation of reliability and repeatability of the substrate; detection of MP by high-performance liquid chromatography (PDF)

Video S1 − Process for extraction of methyl parathion from fruit peels (MP4)

AUTHOR INFORMATION

Corresponding Authors

Jun Zhou − *Department of Microelectronic Science and Engineering, School of Physical Science and Technology, Ningbo University, Ningbo 315211, People's Republic of China*; orcid.org/0000-0003-0346-1390; Email: zhoujun@nbu.edu.cn

Jiaguang Han − *Centre for Terahertz Waves and College of Precision Instrument and Optoelectronics Engineering, Tianjin University, Tianjin 300072, People's Republic of China; Guangxi Key Laboratory of Optoelectronic Information Processing, School of Optoelectronic Engineering, Guilin University of Electronic Technology, Guilin 541004, People's Republic of China*; Email: jiaghan@tju.edu.cn

Authors

Lu Zhou − *Centre for Terahertz Waves and College of Precision Instrument and Optoelectronics Engineering, Tianjin University, Tianjin 300072, People's Republic of China; Department of Microelectronic Science and Engineering, School of Physical Science and Technology, Ningbo University, Ningbo 315211, People's Republic of China*

Lauren Pusey-Nazzaro − *Department of Physics, Washington University in St. Louis, St. Louis, Missouri 63130, United States*

Guanhua Ren − *Centre for Terahertz Waves and College of Precision Instrument and Optoelectronics Engineering, Tianjin University, Tianjin 300072, People's Republic of China*

Ligang Chen − *Centre for Terahertz Waves and College of Precision Instrument and Optoelectronics Engineering,*

Tianjin University, Tianjin 300072, People's Republic of China

Liyuan Liu − *Centre for Terahertz Waves and College of Precision Instrument and Optoelectronics Engineering, Tianjin University, Tianjin 300072, People's Republic of China;* orcid.org/0000-0002-7050-3792

Wentao Zhang − *Guangxi Key Laboratory of Optoelectronic Information Processing, School of Optoelectronic Engineering, Guilin University of Electronic Technology, Guilin 541004, People's Republic of China*

Li Yang − *Department of Physics, Washington University in St. Louis, St. Louis, Missouri 63130, United States;* orcid.org/0000-0002-8611-6359

Complete contact information is available at: https://pubs.acs.org/10.1021/acsnano.1c07695

Author Contributions

L.Z. proposed and performed experiments, analyzed data, and wrote and revised the manuscript. L.P. developed DFT calculations and revised the manuscript. G.R., L.C., L.L., and W.Z. contributed to the data interpretation. L.P., L.Z., and L.Y. contributed to simulations. J.Z. and J.H. proposed and supervised the project and revised and determined the manuscript. All authors contributed to interpretation of the results and approved the submitted version.

Notes

The authors declare no competing financial interest.

ACKNOWLEDGMENTS

This work was supported by the National Key Research and Development Program of China (with grant no. 2017YFA0701004), the National Science Foundation of China (grant nos. 62025504, 61875150, 61935015, and 61675104), the Tianjin Municipal Fund for Distinguished Young Scholars (18JCJQJC45600). L.Y. was supported by the National Science Foundation (NSF) grant No. DMR-2124934. The DFT computation resources were provided by the Extreme Science and Engineering Discovery Environment (XSEDE), which was supported by National Science Foundation (NSF) grant No. ACI-1548562. We thank T. Jiang, C. Gu, Y. Ma, Y. Chen (Ningbo University), and C. Liu (Ludwig-Maximilians-Universität München) for discussions.

REFERENCES

(1) Zheng, Y. B.; Payton, J. L.; Chung, C. H.; Liu, R.; Cheunkar, S.; Pathem, B. K.; Yang, Y.; Jensen, L.; Weiss, P. S. Surface-Enhanced Raman Spectroscopy to Probe Reversibly Photoswitchable Azobenzene in Controlled Nanoscale Environments. *Nano Lett.* **2011**, *11* (8), 3447−3452.

(2) Tran, V.; Walkenfort, B.; Konig, M.; Salehi, M.; Schlucker, S. Rapid, Quantitative, and Ultrasensitive Point-of-Care Testing: A Portable SERS Reader for Lateral Flow Assays in Clinical Chemistry. *Angew. Chem., Int. Ed.* **2019**, *58* (2), 442−446.

(3) Zhou, L.; Liu, Y.; Wang, F.; Jia, Z.; Zhou, J.; Jiang, T.; Petti, L.; Chen, Y.; Xiong, Q.; Wang, X. Classification Analyses for Prostate Cancer, Benign Prostate Hyperplasia and Healthy Subjects by SERS-Based Immunoassay of Multiple Tumour Markers. *Talanta* **2018**, *188*, 238−244.

(4) Hu, Y.; Cheng, H.; Zhao, X.; Wu, J.; Muhammad, F.; Lin, S.; He, J.; Zhou, L.; Zhang, C.; Deng, Y.; Wang, P.; Zhou, Z.; Nie, S.; Wei, H. Surface-Enhanced Raman Scattering Active Gold Nanoparticles with Enzyme-Mimicking Activities for Measuring Glucose and Lactate in Living Tissues. *ACS Nano* **2017**, *11* (6), 5558−5566.

(5) Halvorson, R. A.; Vikesland, P. J. Surface-Enhanced Raman Spectroscopy (SERS) for Environmental Analyses. *Environ. Sci. Technol.* **2010**, *44* (20), 7749−7755.

(6) Liu, B.; Han, G.; Zhang, Z.; Liu, R.; Jiang, C.; Wang, S.; Han, M. Y. Shell Thickness-Dependent Raman Enhancement for Rapid Identification and Detection of Pesticide Residues at Fruit Peels. *Anal. Chem.* **2012**, *84* (1), 255−261.

(7) Cui, H.; Li, S.; Deng, S.; Chen, H.; Wang, C. Flexible, Transparent, and Free-Standing Silicon Nanowire SERS Platform for *in Situ* Food Inspection. *ACS Sens.* **2017**, *2* (3), 386−393.

(8) Kneipp, K.; Wang, Y.; Kneipp, H.; Perelman, L. T.; Itzkan, I.; Dasari, R. R.; Feld, M. S. Single Molecule Detection Using Surface-Enhanced Raman Scattering (SERS). *Phys. Rev. Lett.* **1997**, *78* (9), 1667.

(9) Bruno, P. Surface-Enhanced Raman Scattering-Physics and Applications. *Phys. Today* **2006**, *103* (11), 40.

(10) Kambhampati, P.; Child, C. M.; Foster, M. C.; Campion, A. On the Chemical Mechanism of Surface Enhanced Raman Scattering: Experiment and Theory. *J. Chem. Phys.* **1998**, *108* (12), 5013−5026.

(11) Jensen, L.; Aikens, C. M.; Schatz, G. C. Electronic Structure Methods for Studying Surface-Enhanced Raman Scattering. *Chem. Soc. Rev.* **2008**, *37* (5), 1061−1073.

(12) Yang, L.; Jiang, X.; Ruan, W.; Yang, J.; Zhao, B.; Xu, W.; Lombardi, J. R. Charge-Transfer-Induced Surface-Enhanced Raman Scattering on Ag-TiO_2 Nanocomposites. *J. Phys. Chem. C* **2009**, *113* (36), 16226−16231.

(13) Ben-Jaber, S.; Peveler, W. J.; Quesada-Cabrera, R.; Cortés, E.; Sotelo-Vazquez, C.; Abdul-Karim, N.; Maier, S. A.; Parkin, I. P. Photo-Induced Enhanced Raman Spectroscopy for Universal Ultra-Trace Detection of Explosives, Pollutants and Biomolecules. *Nat. Commun.* **2016**, *7*, 12189.

(14) Zhou, L.; Zhou, J.; Lai, W.; Yang, X.; Meng, J.; Su, L.; Gu, C.; Jiang, T.; Pun, E. Y. B.; Shao, L.; Petti, L.; Sun, X. W.; Jia, Z.; Li, Q.; Han, J.; Mormile, P. Irreversible Accumulated SERS Behavior of the Molecule-Linked Silver and Silver-Doped Titanium Dioxide Hybrid System. *Nat. Commun.* **2020**, *11* (1), 1785.

(15) Han, D.; Yao, J.; Quan, Y.; Gao, M.; Yang, J. Plasmon-Coupled Charge Transfer in FSZA Core-Shell Microspheres with High SERS Activity and Pesticide Detection. *Sci. Rep.* **2019**, *9* (1), 13876.

(16) Praveena, R.; Sameera, V. S.; Mohiddon, M. A.; Krishna, M. G. Surface Plasmon Resonance, Photoluminescence and Surface Enhanced Raman Scattering Behaviour of Ag/ZnO, ZnO/Ag and ZnO/Ag/ZnO Thin Films. *Phys. B* **2019**, *555*, 118−124.

(17) Otto, A. The 'Chemical' (Electronic) Contribution to Surface-Enhanced Raman Scattering. *J. Raman Spectrosc.* **2005**, *36* (6−7), 497−509.

(18) Ling, X.; Xie, L.; Fang, Y.; Xu, H.; Zhang, H.; Kong, J.; Dresselhaus, M. S.; Zhang, J.; Liu, Z. Can Graphene Be Used as a Substrate for Raman Enhancement? *Nano Lett.* **2010**, *10* (2), 553−561.

(19) Huang, S.; Ling, X.; Liang, L.; Song, Y.; Fang, W.; Zhang, J.; Kong, J.; Meunier, V.; Dresselhaus, M. S. Molecular Selectivity of Graphene-Enhanced Raman Scattering. *Nano Lett.* **2015**, *15* (5), 2892−2901.

(20) Ananthoju, B.; Biroju, R. K.; Theis, W.; Dryfe, R. A. W. Controlled Electrodeposition of Gold on Graphene: Maximization of the Defect-Enhanced Raman Scattering Response. *Small* **2019**, *15* (48), No. 1901555.

(21) Feng, S.; dos Santos, M. C.; Carvalho, B. R.; Lv, R.; Li, Q.; Fujisawa, K.; Elías, A. L.; Lei, Y.; Perea-López, N.; Endo, M.; Pan, M.; Pimenta, M. A.; Terrones, M. Ultrasensitive Molecular Sensor Using *N*-Doped Graphene through Enhanced Raman Scattering. *Sci. Adv.* **2016**, *2* (7), No. e1600322.

(22) Huh, S.; Park, J.; Kim, Y. S.; Kim, K. S.; Hong, B. H.; Nam, J.-M. UV/Ozone-Oxidized Large-Scale Graphene Platform with Large Chemical Enhancement in Surface-Enhanced Raman Scattering. *ACS Nano* **2011**, *5* (12), 9799−9806.

(23) Yang, L.; Lee, J. H.; Rathnam, C.; Hou, Y.; Choi, J. W.; Lee, K. B. Dual-Enhanced Raman Scattering-Based Characterization of Stem

Cell Differentiation Using Graphene-Plasmonic Hybrid Nanoarray. *Nano Lett.* **2019**, *19* (11), 8138−8148.
(24) Hao, Q.; Morton, S. M.; Wang, B.; Zhao, Y.; Jensen, L.; Jun Huang, T. Tuning Surface-Enhanced Raman Scattering from Graphene Substrates Using the Electric Field Effect and Chemical Doping. *Appl. Phys. Lett.* **2013**, *102* (1), 011102.
(25) Xu, H.; Xie, L.; Zhang, H.; Zhang, J. Effect of Graphene Fermi Level on the Raman Scattering Intensity of Molecules on Graphene. *ACS Nano* **2011**, *5* (7), 5338−5344.
(26) Xu, H.; Chen, Y.; Xu, W.; Zhang, H.; Kong, J.; Dresselhaus, M. S.; Zhang, J. Modulating the Charge-Transfer Enhancement in GERS Using an Electrical Field under Vacuum and an *n*/*p*-Doping Atmosphere. *Small* **2011**, *7* (20), 2945−2952.
(27) Pristinski, D.; Tan, S.; Erol, M.; Du, H.; Sukhishvili, S. *In Situ* SERS Study of Rhodamine 6G Adsorbed on Individually Immobilized Ag Nanoparticles. *J. Raman Spectrosc.* **2006**, *37* (7), 762−770.
(28) Zhang, C.; Jiang, S. Z.; Huo, Y. Y.; Liu, A. H.; Xu, S. C.; Liu, X. Y.; Sun, Z. C.; Xu, Y. Y.; Li, Z.; Man, B. Y. SERS Detection of R6G Based on a Novel Graphene Oxide/Silver Nanoparticles/Silicon Pyramid Arrays Structure. *Opt. Express* **2015**, *23* (19), 24811−24821.
(29) Espid, E.; Taghipour, F. UV-LED Photo-Activated Chemical Gas Sensors: A Review. *Crit. Rev. Solid State Mater. Sci.* **2017**, *42* (5), 416−432.
(30) Ryu, S.; Liu, L.; Berciaud, S.; Yu, Y. J.; Liu, H.; Kim, P.; Flynn, G. W.; Brus, L. E. Atmospheric Oxygen Binding and Hole Doping in Deformed Graphene on a SiO_2 Substrate. *Nano Lett.* **2010**, *10* (12), 4944−51.
(31) Ratinac, K. R.; Yang, W.; Ringer, S. P.; Braet, F. Toward Ubiquitous Environmental Gas Sensors-Capitalizing on the Promise of Graphene. *Environ. Sci. Technol.* **2010**, *44* (4), 1167−1176.
(32) Brunauer, S.; Deming, L. S.; Deming, W. E.; Teller, E. On a Theory of the van der Waals Adsorption of Gases. *J. Am. Chem. Soc.* **1940**, *62* (7), 1723−1732.
(33) Zhou, Y.; Gao, C.; Guo, Y. UV Assisted Ultrasensitive Trace NO_2 Gas Sensing Based on Few-Layer MoS_2 Nanosheet-ZnO Nanowire Heterojunctions at Room Temperature. *J. Mater. Chem. A* **2018**, *6* (22), 10286−10296.
(34) Rathi, K.; Pal, K. Wireless Hand-Held Device Based on Polylactic Acid-Protected, Highly Stable, CTAB-Functionalized Phosphorene for CO_2 Gas Sensing. *ACS Appl. Mater. Interfaces* **2020**, *12* (34), 38365−38375.
(35) Fan, X.; Elgammal, K.; Smith, A. D.; Östling, M.; Delin, A.; Lemme, M. C.; Niklaus, F. Humidity and CO_2 Gas Sensing Properties of Double-Layer Graphene. *Carbon* **2018**, *127*, 576−587.
(36) Barros, E. B.; Dresselhaus, M. S. Theory of Raman Enhancement by Two-Dimensional Materials: Applications for Graphene-Enhanced Raman Spectroscopy. *Phys. Rev. B: Condens. Matter Mater. Phys.* **2014**, *90* (3), 035443.
(37) Duong, D. L.; Han, G. H.; Lee, S. M.; Gunes, F.; Kim, E. S.; Kim, S. T.; Kim, H.; Ta, Q. H.; So, K. P.; Yoon, S. J.; Chae, S. J.; Jo, Y. W.; Park, M. H.; Chae, S. H.; Lim, S. C.; Choi, J. Y.; Lee, Y. H. Probing Graphene Grain Boundaries with Optical Microscopy. *Nature* **2012**, *490* (7419), 235−239.
(38) Mitoma, N.; Nouchi, R.; Tanigaki, K. Photo-Oxidation of Graphene in the Presence of Water. *J. Phys. Chem. C* **2013**, *117* (3), 1453−1456.
(39) Li, P.; Zhu, L.; Ma, C.; Zhang, L.; Guo, L.; Liu, Y.; Ma, H.; Zhao, B. Plasmonic Molybdenum Tungsten Oxide Hybrid with Surface-Enhanced Raman Scattering Comparable to That of Noble Metals. *ACS Appl. Mater. Interfaces* **2020**, *12* (16), 19153−19160.
(40) Wang, X.; Shi, W.; Wang, S.; Zhao, H.; Lin, J.; Yang, Z.; Chen, M.; Guo, L. Two-Dimensional Amorphous TiO_2 Nanosheets Enabling High-Efficiency Photoinduced Charge Transfer for Excellent SERS Activity. *J. Am. Chem. Soc.* **2019**, *141* (14), 5856−5862.
(41) Teguh, J. S.; Liu, F.; Xing, B.; Yeow, E. K. Surface-Enhanced Raman Scattering (SERS) of Nitrothiophenol Isomers Chemisorbed on TiO_2. *Chem. - Asian J.* **2012**, *7* (5), 975−981.
(42) Lee, D.; Lee, S.; Seong, G. H.; Choo, J.; Lee, E. K.; Gweon, D.-G.; Lee, S. Quantitative Analysis of Methyl Parathion Pesticides in a Polydimethylsiloxane Microfluidic Channel Using Confocal Surface-Enhanced Raman Spectroscopy. *Appl. Spectrosc.* **2006**, *60* (4), 373−377.
(43) Wang, P.; Wu, L.; Lu, Z.; Li, Q.; Yin, W.; Ding, F.; Han, H. Gecko-Inspired Nanotentacle Surface-Enhanced Raman Spectroscopy Substrate for Sampling and Reliable Detection of Pesticide Residues in Fruits and Vegetables. *Anal. Chem.* **2017**, *89* (4), 2424−2431.
(44) Shrivastava, A.; Gupta, V. Methods for the Determination of Limit of Detection and Limit of Quantitation of the Analytical Methods. *Chronicles of Young Scientists* **2011**, *2* (1), 21.
(45) Berrada, H.; Fernández, M.; Ruiz, M. J.; Moltó, J. C.; Mañes, J.; Font, G. Surveillance of Pesticide Residues in Fruits from Valencia during Twenty Months (2004/05). *Food Control* **2010**, *21* (1), 36−44.
(46) Kern, W. Cleaning Solution Based on Hydrogen Peroxide for Use in Silicon Semiconductor Technology. *RCA review* **1970**, *31*, 187−205.
(47) Shim, J.; Yun, J. M.; Yun, T.; Kim, P.; Lee, K. E.; Lee, W. J.; Ryoo, R.; Pine, D. J.; Yi, G. R.; Kim, S. O. Two-Minute Assembly of Pristine Large-Area Graphene Based Films. *Nano Lett.* **2014**, *14* (3), 1388−1393.
(48) Bekki, S.; Vignes-Adler, M.; Nakache, E.; Adler, P. M. Solutal Marangoni Effect: I. Pure Interfacial Transfer. *J. Colloid Interface Sci.* **1990**, *140* (2), 492−506.
(49) Li, X.; Yang, T.; Yang, Y.; Zhu, J.; Li, L.; Alam, F. E.; Li, X.; Wang, K.; Cheng, H.; Lin, C.-T.; Fang, Y.; Zhu, H. Large-Area Ultrathin Graphene Films by Single-Step Marangoni Self-Assembly for Highly Sensitive Strain Sensing Application. *Adv. Funct. Mater.* **2016**, *26* (9), 1322−1329.
(50) Kresse, G.; Furthmuller, J. Efficient Iterative Schemes for *ab Initio* Total-Energy Calculations Using a Plane-Wave Basis Set. *Phys. Rev. B: Condens. Matter Mater. Phys.* **1996**, *54* (16), 11169−11186.

https://doi.org/10.1021/acsnano.1c07695
ACS Nano 2022, 16, 577−587